

EXPERIMENTAL TESTS AND NUMERICAL MODELING TO IDENTIFY THE ASYMPTOTIC SHEAR-COMPRESSION MODE IIA OF CONCRETE FRACTURE

O. MONTENEGRO^{*}, D. SFER[†], C.M. LÓPEZ^{*} AND I. CAROL^{*}

^{*} Universidad Politécnica de Cataluña (UPC)
Edificio D2, Campus Norte UPC
Gran Capitán s/n, 08034 Barcelona, Spain
e-mail: oscar.montenegro@upc.edu, carlos.maria.lopez@upc.edu, ignacio.carol@upc.edu

[†] Instituto de Estructuras (FACET)
Universidad Nacional de Tucumán, Tucumán, Argentina
e-mail: dsfer@herrera.unt.edu.ar

Key words: Shear–compression crack, Concrete fracture, Zero-thickness interface elements

Abstract: In contrast to tensile fracture, shear compression fracture of concrete has not been treated in depth in the literature, in spite of its practical significance in many situations such as confined pull-out, impact, etc. In this paper, we describe the experimental work carried out at ETSECCPB-UPC in order to elucidate the existence of such second mode of fracture and evaluate the associated fracture energy in combination with advanced numerical modeling. A short cylindrical specimens with coaxial cylindrical notches similar to those proposed by Luong (1990) is introduced in a large-capacity triaxial cell, protected with membranes and subject to different levels of confining pressure prior to vertical loading. The specimens tested show a clear shear-compression crack that follows the pre-established crack path, which is in itself a significant achievement. Also, the load-displacement curves for various confining pressures seem to follow the expected trend according to the underlying conceptual model. Finally, a numerical model based on the FEM with zero-thickness interface elements is employed to simulate the fracture initiation and development process, and to identify the fracture parameters including the fracture energies in modes I and IIa out of the experimental curves.

1 INTRODUCTION

Numerous papers in the literature of concrete deal with formulations for the analysis of concrete specimens or structures subjected to mode I fracture processes including the corresponding energy parameter G_f^I . In contrast, mixed mode fracture involving shear and, especially, confined mixed mode fracture under shear-compression, has received much more limited attention.

In 1990 Carol and Prat [1] introduced and later developed [2,3] the concept of asymptotic shear–compression mixed mode or mode IIa, in which very high compression across the

fracture plane prevents any dilatancy and forces the crack to propagate sensibly straight, cutting through aggregates and matrix (figure 1b). In later conference papers, including a previous FRAMCOS conference [4,5] some initial phases of a new experimental program to elucidate the existence of such mode IIa and calibrate the corresponding fracture energy, G_f^{IIa} , were described.

In the current paper, the new results obtained in recent years along this line are presented. The experimental work has been completed, and still on-going numerical studies aim at the full interpretation of those

experimental results.

2 EXPERIMENTAL SETUP

To generate experimentally a shear-compression crack that takes place along a pre-determined plane or surface is not a trivial task. Attempts to modify typical beam-based tensile cracking specimens by applying shear and imposing compression across the fracture plane often lead to deviation of the crack trajectory to a different orientation with lower level of transversal compression. For this purpose, the test setup was developed on the basis of the original specimen proposed by Luong [6,7].

2.1 Specimen geometry

The specimen is a cylinders of 100 mm diameter and 40 mm height, with coaxial 10 mm deep cylindrical notches on both top and bottom faces, which leave between them an also cylindrical notch of height 20mm.

In order to obtain a fracture surface as vertical as possible (given the finite thickness of the notches), upper and lower notches have slightly different diameters, in such way that the outer diameter of the upper notch is as close as possible to the inner diameter of the lower notch. A diagram of the specimens and a transversal cross-section are shown in figure 1.

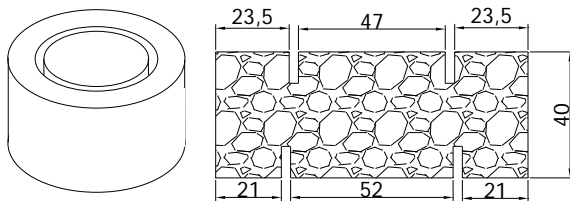


Figure 1: Specimen geometry.

Specimens were cast in cylindrical moulds of 100 mm diameter a 200 mm height. They were then cut in slices and surface ground to 40 mm high, and notches were finally drilled using a special core extraction drill with center-guiding system.

2.2 Loading system

The loading scheme on the specimen is

shown in figure 2, including the lateral pressure on the outer surface of the cylinder providing confinement on the fracture plane, and the special platens top and bottom leading to shearing of the ligament surface.

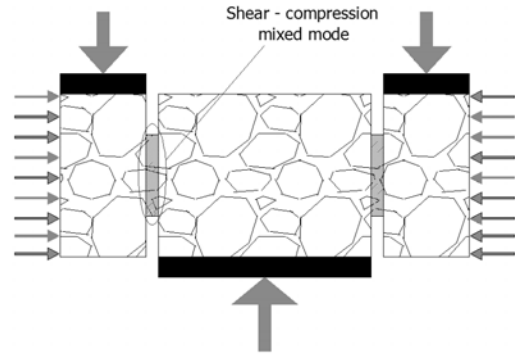


Figure 2: Loading state on specimen (cross-section view).

Except for some basic reference tests performed without lateral pressure, lateral confinement is obtained by introducing the specimen in a large capacity WIKHAM FARRANCE triaxial cell (up to 15x30cm specimens and 140Mpa pressure), as shown in figure 3.

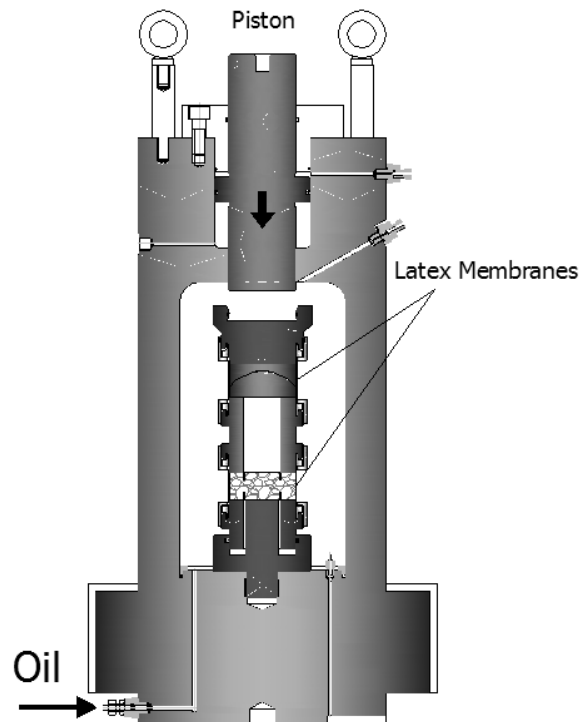


Figure 3: General diagram of confined shear tests.

In pressurized tests, specimens are protected with membranes to isolate them from the confining fluid (oil). Specially designed load platens and other elements shown in figure 3 guarantee post-peak stability of the test and prevent oil penetration along the specimen-platens contact surfaces, among other requirements. More details of the experimental setup can be found in Montenegro et al (2007b).

2.3 Materials

The test series reported corresponds to conventional concrete with uniaxial strength and elastic modulus given in Table 1.

Table 1: Material tested

Material	Max. aggregate size [mm]	f'_c [MPa]	E [MPa]
Conventional Concrete	6	49	25000

At the time of tests, all specimens were older than 28 days.

2.4 Measurement devices

LVDTs are used to measure the relative vertical displacements between load platens, which directly lead to the shear relative displacement along the fracture surface. Because of the confined tests, the LVDTs used were submersible, able to operate under up to 21 MPa of oil pressure inside the triaxial cell. The chamber pressure itself was measured using a pressure transducer.

A specially designed circumferential chain of invariable length with an extensometer transducer between its ends, which can equally operate under oil pressure was used to measure the specimen circumferential deformations.

2.5 Pressure accumulator

The lateral pressure was applied with a manual pump, and was maintained constant during the test by using a pressure accumulator. This consists of a sealed hollow steel cylinder of sufficient volume (figure 4), containing mainly air at the desired pressure

and only a small oil layer at the bottom. The accumulator was connected to the triaxial cell oil circuit though its bottom hose after the circuit had also reached the desired pressure level.

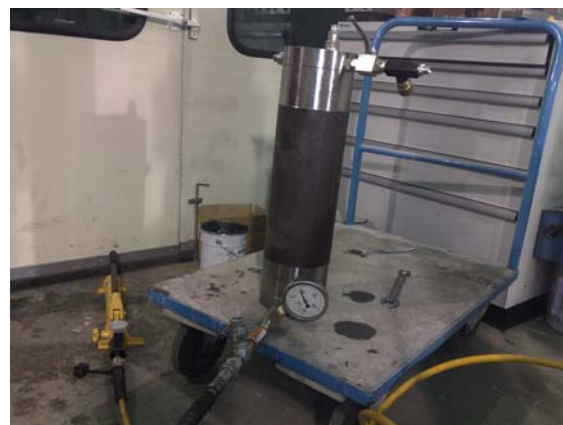


Figure 4: Pressure accumulator device for constant pressure.

2.6 Test sequence

In confined tests, the specimens were subjected first to a lateral confinement pressure which then remained constant during the entire duration of the vertical loading.

Tests were repeated for various levels of lateral confinement pressure, in order to verify the asymptotic character of the shear compression mode of fracture under study.

3 TEST RESULTS

Some preliminary tests with limited or null data acquisition were initially run in order to check the overall performance of the test setup, oil tightness, etc.

Then, various test series were been carried out, some of which are reported here, including one unconfined test and three confined tests at 2, 4 and 8MPa lateral pressure. During those tests, the applied vertical load, and the vertical and circumferential displacements of the specimen were measured.

3.1 Experimental curves

The experimental results are represented in figure5 (rugged curves), together with some

computational simulations explained in Sect. 4 (smooth curves). In the top diagram the curves depict the evolution of the average shear stress transmitted along the ligament (force divided by ligament area, represented on the vertical axis), against the vertical displacement of the top platen which is assumed approximately equal to the average shear relative displacement experienced at the same ligament (horizontal axis). The bottom diagram of the same figure, represents the specimen dilatancy (radial deformation derived from the circumferential deformation, vertical axis) against the same shear displacement as the top diagram.

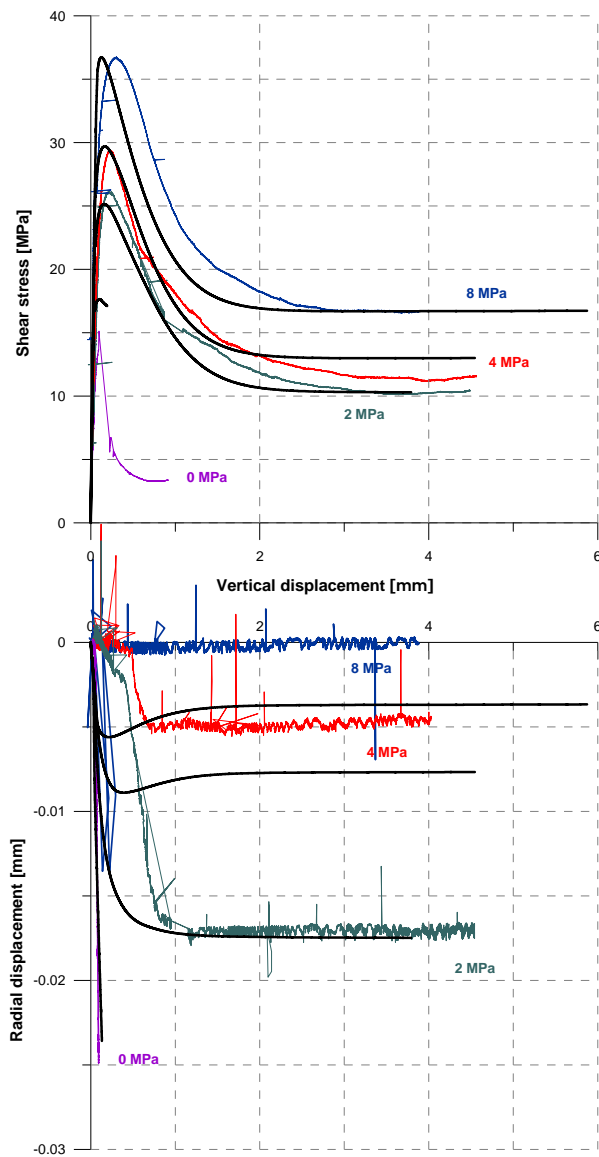


Figure 5: Experimental curves for 2, 4 and 8 MPa confining pressure.

In the curves of figure 5 (top), it can be observed that the unconfined test shows a sharp peak and descending branch, and the test ends at about 1mm shear displacement, while the confined tests have a more round shaped peak and descending branch followed by a clear plateau that is maintained until 4-5 mm. Bottom diagram shows a dilatancy that is very pronounced and actually cannot be measured reliably after the peak for the unconfined peak, while for the confined tests it reaches a clear plateau after about 1mm shear displacement, and its magnitude is drastically decreased to practically zero values for the 8MPa confinement test.

3.2 Cracking observed in specimens

Some images showing the state of the specimens after the test can be observed in figures 6, 7 and 8. Figure 6, shows the tensile radial cracks produced in the unconfined specimen, which are totally developed and in fact the specimen can be physically separated into pieces. The interpretation leads to two phases in the deformation process. First, cracking develops along the cylindrical ligament between the notches, which corresponds to the initial steep part of the post-peak curve in the top diagram of Figure 5. A second mechanism starts operating when this crack is completely developed, and the sliding between the two resulting parts of the specimen begins, because the sliding generates increasing dilatancy which in turn causes the full development of the radial cracks in the outer concrete cylinder. This also helps understanding the difficulties in measuring dilatancy in the test (Figure 5, bottom diagram), since once radial cracks totally formed, the various pieces of the outer ring start moving freely and tend to fall off, only held by the measuring chain device.

In the confined tests, the number and (especially) the opening of tensile radial cracks were significantly reduced with the level of confinement. This is illustrated in Figure 7 showing no visible radial cracks in the 8MPa specimen, in which the outer specimen ring still preserves practically its integrity after the

test.

3.3 Existence of mode IIa (asymptotic mode)

The results obtained clearly seem to indicate the expected trend towards the asymptotic mode IIa previously proposed in a theoretical context (Carol and Prat, 1990, Carol et al. 1997).



Figure 6: State of specimen after the unconfined test, with large fully developed radial cracks.



Figure 7: Radial cracks in a specimen tested under confining pressure of 8 MPa.

Figure 8 depicts the image of a specimen after one of the preliminary tests with a confining pressure of about 4 MPa, which was then cut with a saw in two halves. In the exposed cross-section it can be clearly seen that the fracture plane is produced along an approximately a straight line, cutting through

the aggregates and matrix as expected. In this specimen tensile radial cracks were not appreciated. These observations strongly suggest that in this case the mode IIa was either practically reached or nearly approached. This interpretation is also supported by dilatancy being drastically reduced for tests with confinement of 4MPa, and practically disappearing for 8MPa.



Figure 8: Fracture plane observed in tested specimen, at bottom end observe the displaced aggregate which has been cut through in two pieces by a sensibly straight crack.

4 NUMERICAL MODELING

In parallel to the experimental program described in previous section, a parallel effort has been carried out to simulate numerically the test arrangement and reproduce the results via the FEM with fracture-based zero-thickness interface elements. Taking advantage of symmetry, one fourth of the concrete specimen has been discretized using 3D elements, as shown in Figure 10 (top). The bottom diagram of the same figure, depicts the interface elements that have been introduced along the two major potential fracture surfaces: the cylindrical ligament (in red) and a vertical plane cutting the outer cylinder along a 45 degree line (not colored).

The continuum elements are assumed linear elastic, while the interface elements are equipped with an elasto-plastic fracture-based constitutive law that incorporates G_f^I and G_f^{IIa} as described elsewhere (Carol et al, 1997). The preliminary curves obtained after some

adjustment, for values of the fracture energies of 0.15 and 12 N/mm, are represented in the same diagram as the previous experimental curves (Figure 5). The calculations exhibit general good agreement with the experimental curves, capturing the essential features (peak values, general shape of curves, dilatancy reduction trends, etc.), although some aspects, such as post-peak of the unconfined tests, or dilatancy for high higher confinement still show differences. Ongoing work is aimed at final adjustment process, which depends in part on a new definition of the decay law for dilatancy for the interface constitutive model.

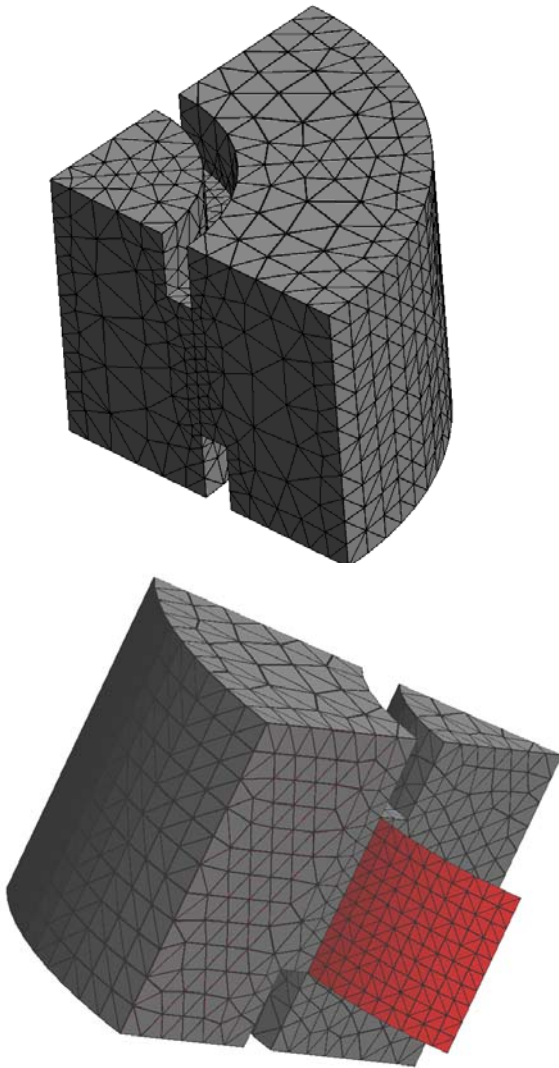


Figure 9: FE mesh (top), and potential fracture planes along which zero-thickness interface elements have been inserted (bottom): along the cylindrical ligament (in red), and also along the exposed vertical face at 45 degree of the top view.

5 CONCLUDING REMARKS

An experimental study has been developed to elucidate the existence of mode IIa in the fracture of concrete specimens. The study was motivated by the previous theoretical developments in the context of a fracture-based constitutive model for the zero-thickness interface element, and has been run in parallel to numerical calculations via FE with zero-thickness interface elements. The calculations have been very useful to understand the stress state occurring in the specimen, and to calibrate the corresponding fracture energy parameter. As the first important achievement, the experiments confirm that a shear-compression crack can be obtained along the pre-determined fracture surface. This is something totally non-trivial and a great success in itself. Additionally, the application of increasing confining pressure seems to lead to the right trend in producing the desired mode IIa crack with no dilatancy. The calculations have led to the right trend for the main variables of the problem, and to relatively good overall adjustment of the curves, for values of G_f^{IIa} about 80 times the classical fracture energy in mode I. This value may seem a little high although it should be taken with care since numerical studies are still on-going and subject to final adjustment of some fine details of the interface constitutive model. In sum, based on the results presented, the experimental/numerical study undertaken seem to confirm the validity of the main concept of the cracking model previously proposed by the authors solely on a theoretical/numerical basis (Carol et al, 1997), and lead to specific values of G_f^{IIa} .

ACKNOWLEDGEMENTS

The research described is partially financed by research grants and BIA2009-10491 and BIA2012-36898 from MEC (Madrid), which include FEDER funds. The group thanks CSIC-Madrid for the consideration as “Unidad Asociada CSIC”. The fourth author also wants to acknowledge the support for his various visits to UPC from grants SGR from AGAUR-Generalitat de Catalunya (Barcelona), in

particular from 2009SGR-180.

REFERENCES

- [1] Carol, I. and Prat, P., 1990. A statically constrained microplane model for the smeared analysis of concrete cracking. In N. Bicanic and H. Mang (eds), *Computer-Aided Analysis and Design of Concrete Structures (Proc. Sci-C 1990)*, Pineridge Press, pp 919-930.
- [2] Carol, I. and Prat, P., 1995. Multicrack model based on the theory of multisurface plasticity and two fracture energies. In Oñate et al, (eds), *COMPLAS4. CIMNE (UPC) Barcelona*, pp 1583-1594.
- [3] Carol, I., Prat, P. and Lopez, C.M., 1997. Normal/shear cracking model: Application to discrete crack analysis. *Journal of Engineering Mechanics*. **123**, No.8, pp. 765-773.
- [4] Montenegro, O., Carol, I., Sfer, D., 2007. Characterization of confined mixed-mode fracture in concrete. In Carpieneri et al (eds), *Fracture Mechanics of Concrete and Concrete Structures (FRAMCOS 6)*, June 17-22, 2006, Catania, Italy; pp, 257-261.
- [5] Montenegro, O., Sfer, D., Carol, I., 2007. Characterization of concrete in mixed mode fracture under confined conditions. In Gdoutos, E.E., editor, *Experimental analysis of nano and engineering material and structures*, pp. 1–8. Springer. (Proc. of the 13th Int. Conf., Alexandroupolis, Jul/1-6/2007) – in CD-ROM.
- [6] Luong, M.P., 1990. Tensile and shear strength of concrete and rock. *Engineering Fracture Mechanics*. **35**, N°1/2/3, pp 127-135.
- [7] Luong, M.P., 1992. Fracture testing of concrete and rock materials. *Nuclear Engineering and Design*. **133**, pp 83-95.